Nucl. Sci. and Tech., Vol.12, No. 3 (2022), pp. 11-20

Nuclear Science and Technology

Journal homepage: http://jnst.vn/index.php/nst

Detector corrections for particle identification in SAMURAI spectrometer

N. D. Ton[1], B. D. Linh[2], Seastar3 collaborator

[1] *Institute for Nuclear Science and Technology, 179 Hoang Quoc Viet, Cau Giay, Ha Noi*
[2] *Vietnam Agency for Radiation and Nuclear Safety, 14th floor, 113 Tran Duy Hung, Cau Giay, Ha Noi*
Email: nguyenducton92@gmail.com

Abstract: **S**uperconducting **A**nalyzer for **MU**lti particles from **Ra**dio **I**sotope beams (SAMURAI) is an advanced spectrometer at RIKEN for experiments in which complete kinematic is determined to derive invariant-mass spectroscopy and parallel momentum distribution. This report represents the basic structure and technical advantages of SAMURAI, which was utilized in the third campaign of the "*Shell Evolution An Search for Two-plus energies At RIBF*" (SEASTAR3) project. In adition, corrections for particle identification at the SAMURAI will be discussed. These corrections are a typical and crucial step in the data analysis process in SEATAR3 experiments. The particle identification results will be used for further analysis of the properties of nuclear structure of neutron-rich nuclei around N = 32, 34.

Keywords: *SEASTAR, particle identification, BigRIPS, SAMURAI.*

I. INTRODUCTION

The structure of nuclei close to stability has been well described by the nuclear shell model and characterized by single-particle orbitals grouped in energy shells, separated by energy gaps. Nuclei with a completely filled shell of protons and/or neutrons are called "magic nuclei" and represent the backbone of nuclear structure physics. Recently, since the availability of radioactive ion beams (RIBs), research on unstable nucleon-rich nuclei has attracted much more attention. Novel phenomena such as halo structure and neutron skin [1, 2], intruder states [3, 4], and the appearance of new magic numbers [5], which are beyond the explanation of the shell model, i.e., were discovered. Recent investigations on exotic nuclei near the drip line have revealed that the magic numbers may change locally, leading to the disappearance of shell gaps and the appearance of new magic numbers. Some pieces of evidence of the disappearance of the "magic number" N = 28 in the ^{42}Si [6] and/or appearance of the new magic number N = 16 in ^{24}O [7,8], N = 34 in ^{54}Ca nuclei [9, 10] have been reported. Moreover, the robustness of a new sub-shell closure at N = 32 below the proton magic number Z = 20 has been highlighted [11, 12]. In the region Z below 20 with N ≥ 28, the theoretical calculations [5, 13-16] in the *sd-pf* valence space predict the restoration of $J^{\pi} = 3/2^{+}$ ground state due to the filling of $\nu 1p_{3/2}$ orbital and repulsive $\pi 0d_{3/2}$-$\nu 1p_{3/2}$ versus attractive $\pi 1s_{1/2}$-$\nu 1p_{3/2}$ mono-pole interactions. However, there is no available data for this region. In addition, the nuclear structure properties of neutron-rich nuclei around the ^{54}Ca: local of the neutron in *pf* shell around N = 34; the correlation between structures of Ca isotopes which is heavier than ^{54}Ca [17]; the

https://doi.org/10.53747/nst.v12i3.343
Received 25 November 2022, accepted 08 May 2023

range of “island of inversion” N = 40 is an exciting subject.

In the previous campaigns of the SEASTAR experiment, the combination of the MINOS target and DALI2 detector, ZeroDegree spectrometer [19] allowed us to measure the gamma-ray spectra of neutron-rich nuclei. Consequently, new structure data of neutron-rich nuclei around the drip line had been achieved by analyzing the gamma-ray spectra of interesting nuclei. Even though, valuable data such as orbital angular momenta of removed nucleon or unbound state in exotic nuclei have not been achieved due to the limitation of the detectors. Therefore, SAMURAI (Superconducting Analyzer for MUlti particles from Radio Isotope beams) [18] was designed and utilized in the third campaign of the SEASTAR experiments. The SAMURAI spectrometer was designed to optimize the coincidence measurement between heavy projectile fragments and projectile-rapidity neutrons/protons with significant angular and momentum acceptance [18]. Besides the particle identification role, SAMURAI allows us to analyze the inclusive parallel-momentum distribution (PMD) and invariant-mass spectroscopy of the residual nuclei by using a dipole magnet and two neutron detectors. These mentioned data could be used to assign the orbital angular momenta of the removed nucleon (l = 0, 1, or 2) or investigate the unbound state in exotic nuclei, respectively. Because of that, it allows measurements of reactions with unbound states and studies on the properties of the unbound excited states and those of the ground state of nuclei away from the stability valley on both the neutron- and proton-rich sides.

The SAMURAI spectrometer was used in the third campaign of the SEASTAR project, which contributed significantly to the success of the results of the study of the nuclear structure of neutron isotopes in the SEASTAR3 experiment [20-24]. One of the important donations of SAMURAI is particle identification after the reaction in the secondary target. This report presents the basic design of SAMURAI. Besides, the procedure of corrections for particle identification will be discussed with an example of particle identification for ^{50}Ar(p,2p)^{49}Cl reaction. Two main corrections consisting of slew and alignment corrections have been suggested to optimize the PID results. The correct results of PID at SAMURAI are crucial data to determine the proper reaction channels and could be used to remove the background and noise of the gamma spectrum.

II. SBT AND HODF CORRECTION

A. SAMURAI setup

The SAMURAI spectrometer was designed as a large-acceptance spectrometer for RIB experiments and used to identify and analyze the production of reactions at the MINOS target [25]. It consists of a superconducting magnet with a large vacuum chamber and is surrounded by beam-line detectors for neutron and charged particles. One of three different exit branches from the BigRIPS separator beam line is connected to the SAMURAI spectrometer. The schematic layout of the SAMURAI is shown in Figure 1. Similar to the BigRIPS separator, SAMURAI used the TOF-Bρ-ΔE method to identify neutron-rich nuclei [18]. In order to measure the timing and position information of the incident beam, plastic scintillators (SBTs) [18] and tracking detectors (BDC1 and BDC2) [18] were installed (see Fig. 1). By that way, SAMURAI allows to determine the momentum vector of the incoming beam.

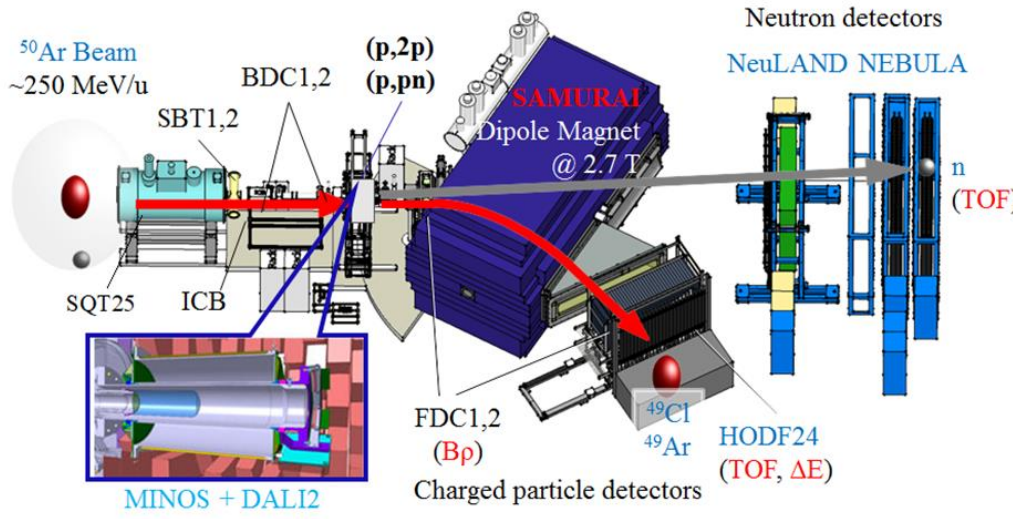

Fig. 1. Schematic view of the SAMURAI setup for the third SEASTAR campaign. Two red arrows and the gray arrow show the trajectories of a ^{50}Ar beam particle, a heavy fragment ^{49}Cl, and neutrons (knocked-out and decay neutrons), respectively. See the text for details. Image modified from [26]

The isotopes of interest (^{50}Ar) were separated and focused before impinging on the MINOS LH_2 (liquid hydrogen) target to induce a knock-out reaction. Around the MINOS, the DALI2+ array [27, 28] was installed to detect prompt gamma-ray emitted from residual particles ^{49}Cl in the very forward directions. Besides, as an intrinsic property of neutron-rich nuclei, ^{49}Cl could decay to ^{48}Cl and release a neutron. At the exit of MINOS, a superconducting dipole magnet (the SAMURAI magnet) was used to separate charged particles and produced neutrons using an analysis of the rigidity. Then, particle identification parameters were measured by beamline detectors such as FDC and HODF24 [18]. For that purpose, magnet rigidity (Bρ) was determined by the trajectory information from FDC1 and FDC2 integrating with transfer matrix elements of the magnet [18], while ΔE and TOF were determined by HODF24. Then, the atomic number (Z) and charge-over-mass ratio (A/Q) of the particles would be deduced based on Bρ-ΔE-TOF method. Furthermore, the momentum vector of the heavy fragments could be determined from their trajectory data. Likewise, the momentum vector of the decaying neutron was measured by using two neutron detector arrays - NeuLAND [29] and NEBULA [18] (Fig. 1).

For more details, an example of ^{50}Ar(p,2p)^{49}Cl reaction channel will be discussed. The ^{49}Cl fragments were produced from the interaction between ^{50}Ar projectiles and the LH_2 target. Then, the identification step at the SAMURAI was performed based on the TOF-Bρ-ΔE method. While magnetic rigidity (Bρ) was determined by the trajectory information from FDC1 and FDC2 integrating with transfer matrix elements of the magnet [18], ΔE and TOF were measured by HODF24. Logic signals from SBT detectors at F13 were used to determine the timing in the SAMURAI spectrometer and the beam trigger. Therefore, the SAMURAI particle identification is very sensitive to SBT measured time effect. A calibration was performed during the experiment to obtain a preliminary PID (online result). However, the correlation between the atomic number (Z) versus mass-to-charge ratio (A/Q) does not show the correct A/Q and the best resolution values. Thus, particle

identification correction is a necessary step. Figure 2 presents online PID in SAMURAI. In this figure, the A/Q of ^{49}Cl appears to be 2.89 instead of the expected value of 2.882 (49/17), and the corresponding resolution σ was 0.0076 (see panel b of Fig. 2).

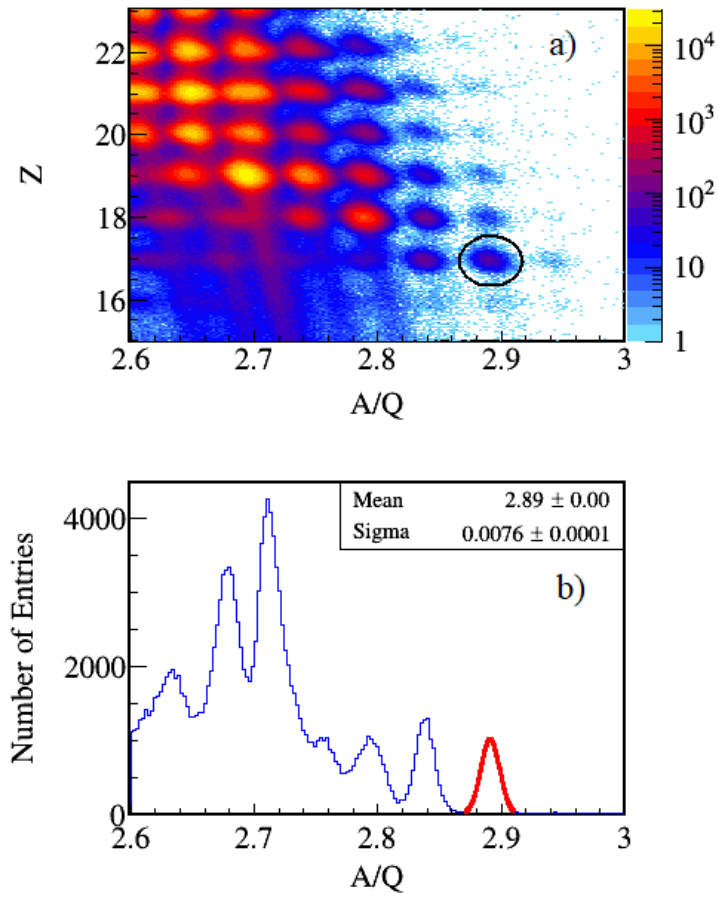

Fig. 2. a) - Online PID, Z vs. A/Q.^{49}Cl was marked in the black ellipse. b) – A projection on the A/Q axis of K isotopes. The red line is a fit using the Gaussian function to get the resolution for ^{49}Cl. (replace with the new one)

The SBT1 and SBT2 are two thin plastic scintillators located about 2.7 m upstream from the LH_2 target (see Fig. 1). At the left (L) and right (R) ends of each SBT concerning the beam direction, two photomultiplier tubes (PMT) were attached. PMT signals were split into three parts: one signal was sent to QDC (Charge to Digital Converter), and the others were sent to discriminators to generate logic signals. The schematic layout of the SBT is given in Figure 3(a). To measure the TOF and energy loss, a HODF24 which consists of 24 bars of plastic scintillation, was installed after the FDC2. It was used for detecting charged fragments from the target. Signals from the separated bar were read out by two PMTs at the ends of individual one (both up (U) and down (D) sides). The anode signals from the PMTs were split and sent to the QDC and the leading-edge discriminator. The schematic view of the HODOF4 is given in Figure 3(b).

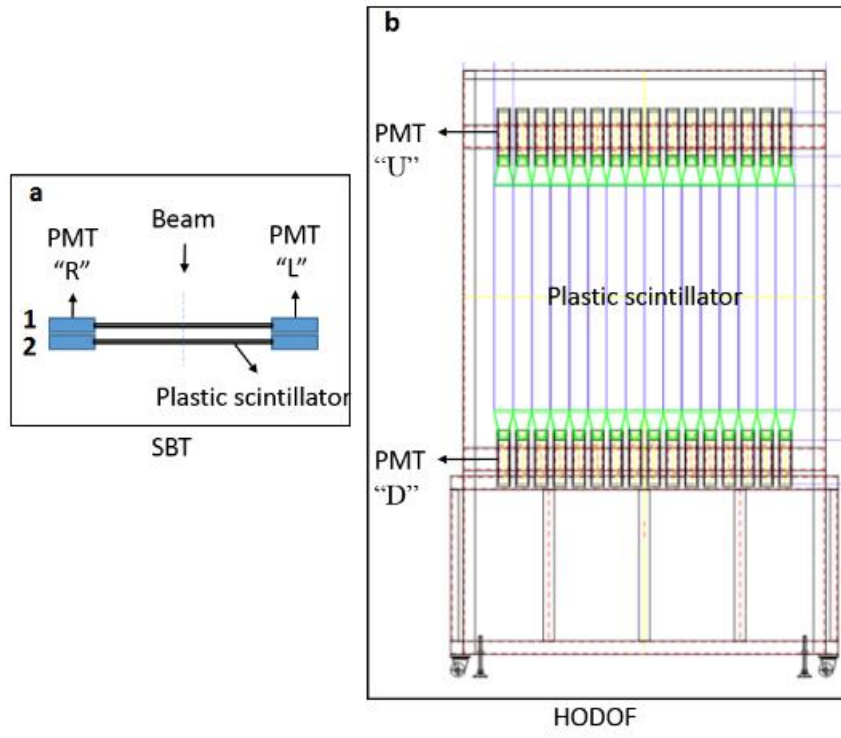

Fig. 3. The schematic view of SBT (a) and HODOF (b)

B. Data corrections

As mentioned earlier, particle identification correction at the SAMURAI is needed for data analysis. Typically, it consists of two main corrections: slew and alignment correction. In the below parts, the procedure for these corrections will be discussed.

1. Slew correction

Due to the time dependence on pulse height in leading-edge discriminators, the walking effect (or slew effect) refers to the dependence of the generated time signal on the amplitude. It comes directly from the method used to discriminate signals. When a fixed threshold as a discriminator applies two signals with different amplitudes but coincident in time, these will be triggered at other times due to the difference in the pulse height. Although the slewing effect worsens the time resolution, photons are particularly suitable as a correction tool because their velocity is unchanged at any energy. In both SBT and HODF24, the timing information was corrected using the light output information in order to compensate for this effect. Time-light output correction was performed by applying a phenomenological function of charge discussed in Ref. [30]. Figure 4 compares the time-light output correlation at the SBT1 before and after correction. Where F13_1_Time = (F13Pla_1_TL + F13Pla_1_TR)/2 and F13_2_Time = (F13Pla_2_TL + F13Pla_2_TR)/2 are the time of each SBT detector. F13Pla_1_TL, F13Pla_1_TR, F13Pla_2_TL, F13Pla_2_TR, F13Pla_1_QL, F13Pla_1_QR, F13Pla_2_QL, F13Pla_2_QR represent the measured time (T), the measured light output (Q) of the left (L) and right (R) of SBT, respectively. The time resolution was achieved by applying a Gaussian fitting, as shown on panels (c) and (d) of Figure 4. The result is consistent with the previous report [23].

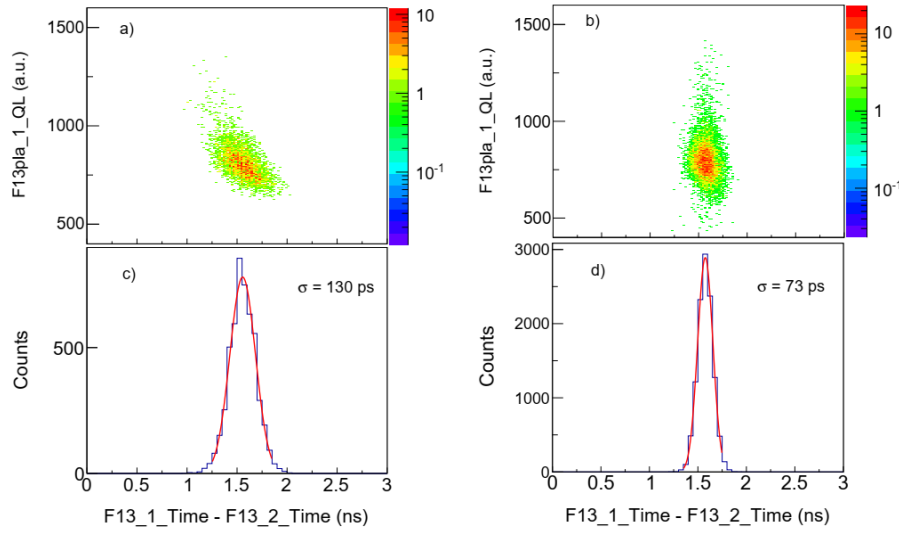

Fig. 4. Upper panels: Timing and light output correlation of SBT1 without (a) and with (b) the slew correction for ^{50}Ar isotope. F13Pla_1_QL and F13Pla_1_QR represent the measured light output (Q) of the left (L) and right (R) of SBT1, respectively. Lower panels: The projection of the time differences between SBT1 and SBT2 on the horizontal axis without (c) and with (d) the slew correction. The red lines are the fit using Gaussian functions to get the resolution. F13_1_Time and F13_2_Time are the time of each SBT detector

Similarly, slew correction in HODF24 was also performed and the result was shown in Figure 5. The procedure slightly changed according to each upside and downside of the HODF24 bars.

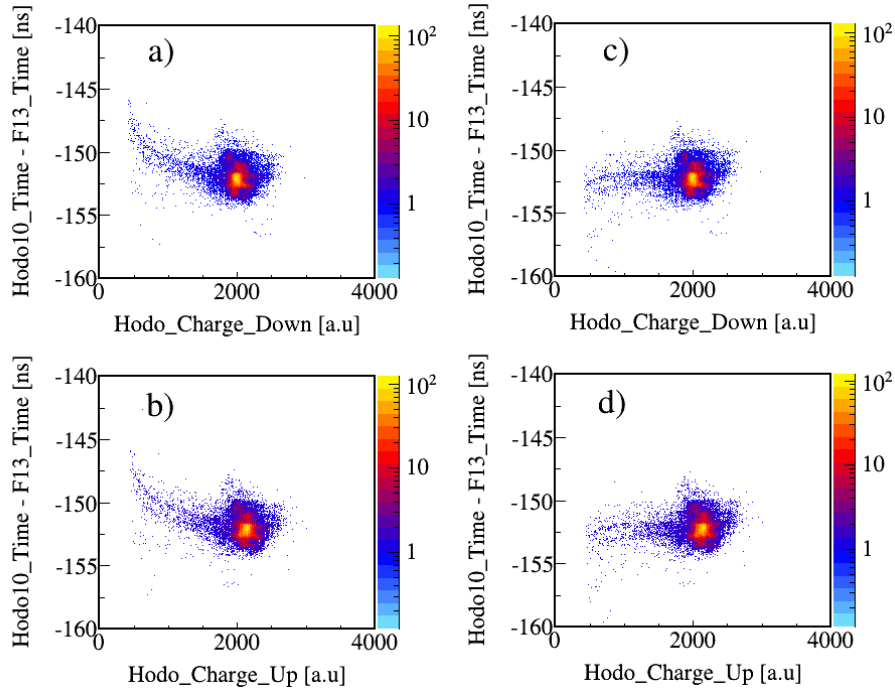

Fig. 5. Correlation of charge and a different time in 10th HODF24 bar and SBT. a) - charge measure at downside without slew correction; b) - charge measure at upside without slew correction; c) - charge measure at downside with slew correction; d) - charge measure at upside with slew correction

2. Alignment correction

During experiments, because of some unexpected effects, such as temperature fluctuation and the shifting of detector thresholds, incorrect data were recorded. Ideally, the initial thresholds should be kept as constants, but unfortunately, these mentioned effects randomly occurred. Because of that, a correction procedure would be applied in 2 scales: event-by-event for each run and, afterward, applied for different runs (run by run). For example, figure 6-a) shows the variances of measured charge on the left side of SBT1 in a typical run. Similarly, the top left and top right panels of figure 7 show the difference in charge and time on the 15th bar of HODF24 in different runs. The method to align the signal is as follows:

+ For individual run (event-by-event): five isotopes with high statistics such ^{50}Ar, ^{49Cl}, ^{53}Ca, ^{56}Sc, and ^{60}Ti in BigRIPS were selected then their data would be used as a reference to build the correlation between light output at the left side of F13 (F13_1_QL) and event number. Data of each isotope were binned into small parts, which consisted of 1000 events. Then, the correlation between F13_1_QL and the event number of the first of 1000 events was taken as a reference, and data in other bins should be aligned. According to 5 data points corresponding to 5 isotopes for each ith bin, two coefficients were obtained using a linear fitting: y = p1 * x + p2 through those 5 data points, then applied to perform the alignment for the whole run data. Figures 6.a and 6.b compare the charge distribution at the left side of SBT1 before and after alignment correction.

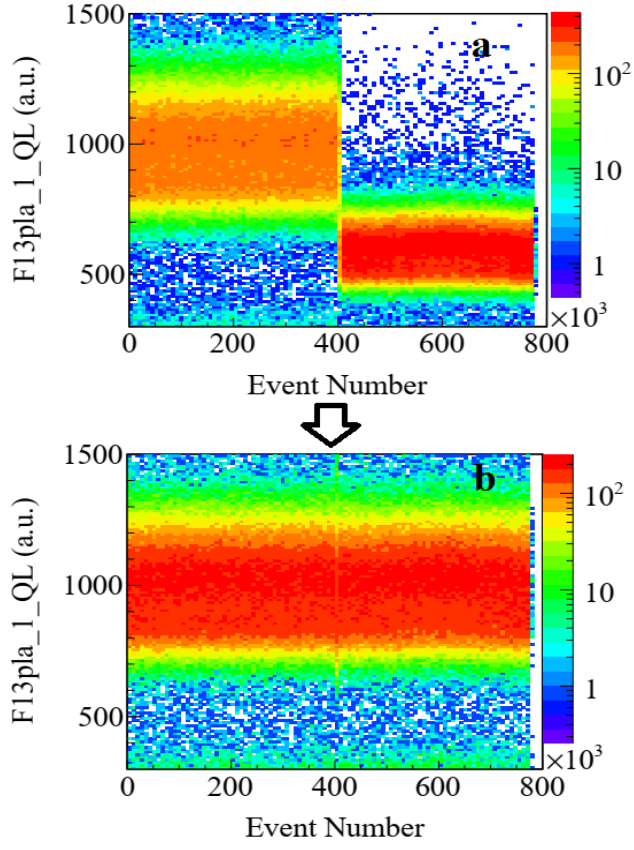

Fig. 6. An example of the alignment result for a typical run. Correlation plots between event number and light output before (a) and after (b) correction

+ The alignment correction for the whole experiment data was performed in a similar way as the correction for the individual run. There are two corrections in this step: charge and time alignment. For charge alignment, the collected charge of the plastics for a typical run was taken as a reference, and then other plastics were aligned to this reference. For example, the beam of ^{61}V was chosen as a Z reference for the 15th bar (ID = 15) and shown in Figure 7. A linear correction was performed to refer to a typical run. The bottom left panel of figure 7 shows the charge alignment result after applying the correction parameters, while the top left panel shows the original one. In the same way, time alignment was performed, and the obtained results are shown in the right panel of Figure 7. The top right panel and the bottom right panel of Figure 7 present the HODF24 time before and after alignment, respectively. F13 Time value indicates the average measured time in SBT1 and SBT2 detectors.

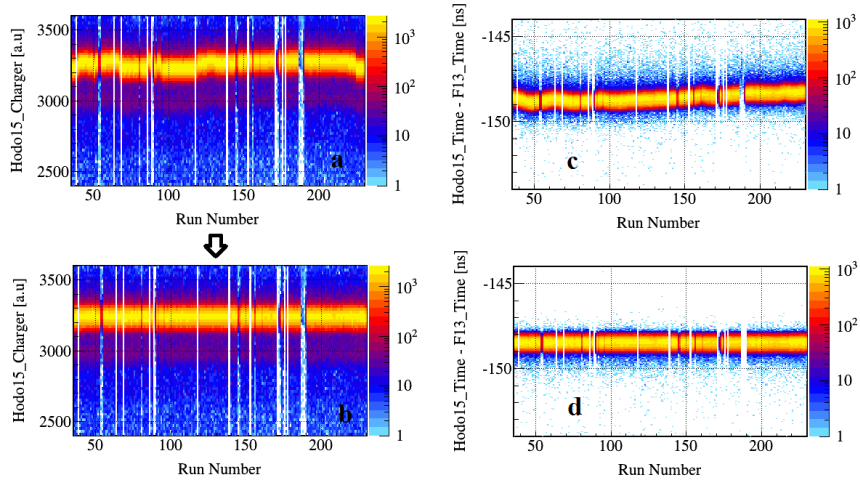

Fig. 7. Correlation between HODF24 charge and run numbers before (a) and after (b) alignment. A different time between HODF24 and SBT versus run numbers correlation before (c) and after (d) alignment. ^{61}V beam were choose as Z reference for 15th bar (bar 15/24th of HODF)

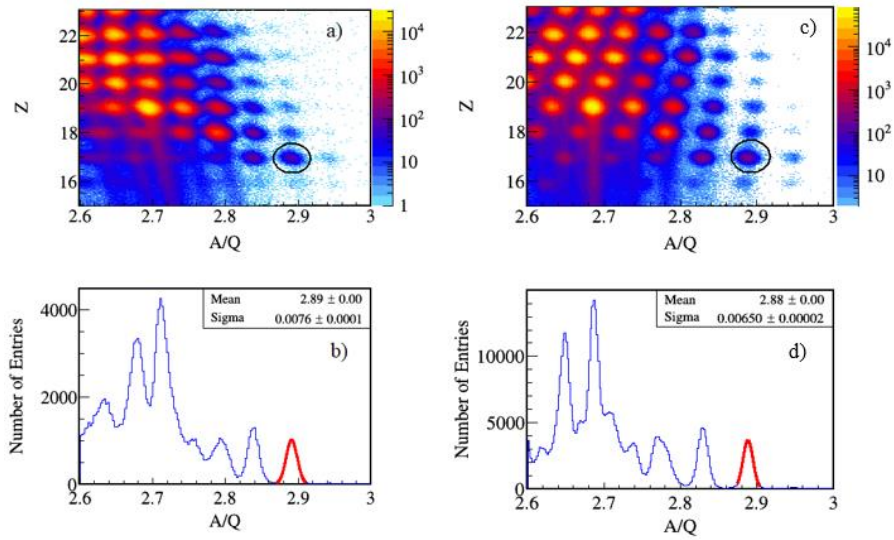

Fig. 8. Online particle identification of atomic number (Z) vs. mass-to-charge ratio (A/Q) in SAMURAI with all experiment data with (right panels) and without (left panels) correction. ^{49}Cl was marked in the black ellipse. The bottom panels show A/Q projection for Cl isotopes. The red lines indicate the fit using Gaussian functions to get the resolution for ^{49}Cl

By applying slew and alignment corrections, the PID plot of atomic number (Z) versus mass-over-charge ratio (A/Q) of residual particles at the SAMURAI was obtained and compared with the uncorrected data, as presented in Figure 8. It shows that after being corrected, the particles of interest were separated more clearly. As an example, the atomic number (Z) and corresponding resolution (σ) of the ^{49}Cl isotope are Z = 17 and 0.79(1)%. Also, the (A/Q) value and corresponding resolutions (σ) before and after corrections are 2.89(0.0076) and 2.88(0.0065) respectively.

III. CONCLUSIONS

The report introduced an overview of SAMURAI – a high-precision spectrometer used for invariant mass and momentum measurements in the third campaign of the SEASTAR project. Also, the procedure of PID corrections - the first step of data analysis at the SAMURAI was described. The quality of PID was estimated by the resolution of Z and A/Q distribution, then the effect of PID corrections was demonstrated by the improvement of PID resolution. These PID results are essential in further studies on the spectroscopy of interested nuclei.

The Vietnamese authors would like to thank VINATOM and the Vietnam Ministry of Science and Technology for the support under Grant No. ĐTCB.01/21/VKHKTHN, Dr. Do Cong Cuong and Dr. Le Xuan Chung at INST for their comments that greatly improved the manuscript.

REFERENCES

[1]. I. Tanihata, "*Neutron halo nuclei*", J. Phys. G **22**, 157, and references therein, 1996.

[2]. L. X. Chung et al., "*Elastic proton scattering at intermediate energies as a probe of the ^{6,8}He nuclear matter densities*", Phys. Rev. C **92**, 034608, 2015.

[3]. S. D. Pain et al., "*Structure of ^{12}Be: Intruder d-Wave Strength at N=8*", Phys. Rev. Lett. **96**, 032502, 2006.

[4]. Le Xuan Chung et al., "*The dominance of the $\nu(0d_{5/2})^2$ configuration in the N = 8 shell in ^{12}Be from the breakup reaction on a proton target at intermediate energy*", Phys. Lett. B **774**, 559–563, 2017.

[5]. O. Sorlin et al., "*Nuclear magic number: New features far from stability*", Progress in Particle and Nuclear Physics **61**, Issue 2, 602-673, 2008.

[6]. Bastin, B. et al., "*Collapse of the N = 28 shell closure in ^{42}Si*", Phys. Rev. Lett. **99**, 022503, 2007.

[7]. R. Kanungo et al., "One-Neutron Removal Measurement Reveals ^{24}O as a New Doubly Magic Nucleus", Phys. Rev. Lett. 102, 152501, 2009

[8]. C.R. Hoffman et al., "*Evidence for a doubly magic ^{24}O*", Phys. Lett. B **672**,17–21, 2009.

[9]. F. Wienholtz et al., "*Masses of exotic calcium isotopes pin down nuclear forces*," Nature **498**, 346, 2013.

[10]. D. Steppenbeck et al., "*Evidence for a new nuclear 'magic number' from the level structure of ^{54}Ca*", Nature **502**, 207–210, 2013.

[11]. D. Steppenbeck et al., "*Low-Lying Structure of ^{50}Ar and the N = 32 Subshell Closure*", Phys. Rev. Lett. **114**, 252501, 2015.

[12]. M. Rosenbusch et al., "*Probing the N = 32 Shell Closure below the Magic Proton Number Z = 20: Mass Measurements of the Exotic Isotopes ^{52,53}K*", Phys. Rev. Lett. **114**, 202501, 2015.

[13]. J. Retamosa et al., "*Shell model study of the neutron-rich nuclei around N= 28*", Phys. Rev. C **55**, 1266, 1997.

[14]. S. Nummela et al., "*Spectroscopy of ^{34,35}Si by β decay: sd–fp shell gap and single-particle states*", Phys. Rev. C **63**, 044316, 2001.

[15]. F. Nowacki et al., "*New effective interaction for 0ħω shell-model calculations in the sd−pf valence space*", Phys. Rev C **79**, 014310, 2009.

[16]. A. Gade et al., "*Evolution of the $E(1/2^+_1) - E(3/2^+_1)$ energy spacing in odd-mass K, Cl, and P isotopes for N = 20-28*", Phys. Rev. C **74**, 034322, 2006.

[17]. M. Honma et al., "*Effective interaction for pf-shell nuclei*", Phys. Rev. C **65**, 061301, 2002.

[18]. T. Kobayashi et al., "*SAMURAI spectrometer for RI beam experiments*", Nuclear Instruments and Methods in Physics Research B **317**, 294–304, 2013.

[19]. B. D. Linh et al., "*Particle identification for Z = 25 – 28 exotic nuclei from SEASTAR experimental data*", Nuclear Science and Technology, Vol. **7**, No. 2, pp. 01-07, 2017.

[20]. B. D. Linh et al., "*Investigation of the ground-state spin inversion in the neutron-rich $^{47,49}Cl$ isotopes*," Phys. Rev. C **104**, 044331, 2021.

[21]. M. M. Juhász et al., "*First spectroscopic study of ^{63}V at the N = 40 island of inversion*," Phys. Rev. C **103**, 064308, 2021.

[22]. F. Browne et al., "*Pairing Forces Govern Population of Doubly Magic ^{54}Ca from Direct Reactions*," Phys. Rev. Lett. **126**, 252501, 2021.

[23]. M. M. Juhász et al., "*First spectroscopic study of ^{51}Ar by the (p,2p) reaction,"* Phys. Lett. B **814**, 136108, 2021.

[24]. M. Enciu et al., "*Extended $p_{3/2}$ Neutron Orbital and the N=32 Shell Closure in ^{52}Ca*" Phys. Rev. Lett. **129**, 262501, 2022.

[25]. A. Obertelli et al., "MINOS: A vertex tracker coupled to a thick liquid-hydrogen target for in-beam spectroscopy of exotic nuclei", *Eur. Jour. Phys. A* 50, 8, 2014.

[26]. Z. Yang, F. Marqu†s, *et al., Study of Multi-neutron Systems with SAMURAI Spectrometer*, pp. 529–534. Germany: Springer, 01, 2020.

[27]. I. Murray, F. Browne, *et al.*, "DALI2+ at the RIKEN Nishina Center RIBF," *RIKEN Accelerator Progress Report*, vol. 51, p. 158, 2018.

[28]. S. Takeuchi, "DALI2: A NaI(Tl) detector array for measurements of γ rays from fast nuclei", *Nucl. Instrum. and Methods in Phys. Res. Sect. A*, 763-596, 2014.

[29]. https://www.gsi.de/neuland.

[30]. http://lambda.phys.tohoku.ac.jp/~kobayash/samuraiD/memo/index.html.